PHILOSOPHICAL TRANSACTIONS



rsta.royalsocietypublishing.org

Research



Cite this article: Henkin G, DeCamp SJ, Chen DTN, Sanchez T and Dogic Z. 2014 Tunable dynamics of microtubule-based active isotropic gels. *Phil. Trans. R. Soc. A* **372**: 20140142.

http://dx.doi.org/10.1098/rsta.2014.0142

One contribution of 10 to a Theme Issue 'New trends in active liquid crystals: mechanics, dynamics and applications'.

Subject Areas:

biophysics, fluid mechanics, light microscopy, mechanics

Keywords:

active matter, gels, bundled microtubules, molecular motors, spontaneous flow

Author for correspondence:

Zvonimir Dogic e-mail: zdogic@brandeis.edu

[†]These authors contributed equally to this study.

Electronic supplementary material is available at http://dx.doi.org/10.1098/rsta.2014.0142 or via http://rsta.royalsocietypublishing.org.



Tunable dynamics of microtubule-based active isotropic gels

Gil Henkin^{1,†}, Stephen J. DeCamp^{1,†}, Daniel
T. N. Chen¹, Tim Sanchez² and Zvonimir Dogic¹

¹Department of Physics, Brandeis University, Waltham, MA 02454, USA

²School of Engineering and Applied Sciences, Harvard University, Cambridge, MA 02438, USA

We investigate the dynamics of an active gel of bundled microtubules (MTs) that is driven by clusters of kinesin molecular motors. Upon the addition of ATP, the coordinated action of thousands of molecular motors drives the gel to a highly dynamical turbulent-like state that persists for hours and is only limited by the stability of constituent proteins and the availability of the chemical fuel. We characterize how enhanced transport and emergent macroscopic flows of active gels depend on relevant molecular parameters, including ATP, kinesin motor and depletant concentrations, MT volume fraction, as well as the stoichiometry of the constituent motor clusters. Our results show that the dynamical and structural properties of MT-based active gels are highly tunable. They also indicate existence of an optimal concentration of molecular motors that maximize far-from-equilibrium activity of active isotropic MT gels.

1. Introduction

The laws of equilibrium statistical mechanics impose severe constraints on the properties of conventional materials assembled from inanimate building blocks. Consequently, such materials cannot exhibit spontaneous motion or perform macroscopic work. Inspired by inherently far-from-equilibrium biological phenomena such as collective dynamics of a flock of birds, travelling metachronal waves of dense ciliary fields or spontaneous streaming flows of a cellular cytoplasm, recent efforts

have focused on recreating diverse biological functionalities in highly simplified materials [1-7]. Being recreated from the bottom up, the dynamical properties of these active materials are highly tunable, making them suitable for rigorously testing rapidly developing theoretical models of active matter [8-12], as well as their use in potential applications. In particular, recent experiments have shown that in the presence of attractive depleting interactions, short microtubule (MT) filaments assemble into three-dimensional isotropic gels that exhibit persistent spontaneous flows, enhanced transport and self-mixing [13]. In contrast to conventional systems where flows are induced by inputting energy at the macroscopic scale, macroscopic flows of MT-based active gels are driven by coordinated activity of thousands of microscopic kinesin molecular motors. We systematically vary relevant microscopic parameters of active gels and determine how these affect the emergent large-scale spontaneous flows. Our results demonstrate that the average speed at which the active gel spontaneously flows can be tuned by orders of magnitude. They also demonstrate that it is possible to systematically tune the spatial properties of active gels, such as the average vorticity lengthscale. Finally, they strongly suggest that there is an optimal concentration of molecular motors that maximize the emergent flows of active gels. Increasing the number of motors beyond this optimal number leads to internal frustrations that significantly slow down the overall gel dynamics.

(a) Active isotropic gels

The three essential building blocks of active isotropic gels are filamentous MTs, clusters of kinesin molecular motors, and a depletion agent polyethylene-glycol (PEG; figure 1). MT filaments are stabilized by GMPCPP, a non-hydrolysable analogue of guanosine-5'-triphosphate (GTP) which suppresses dynamical instability and turnover of tubulin monomers [14]. Guanosine $5'-(\alpha,\beta-methylenetriphosphate)$ (GMPCPP) also significantly lowers the nucleation barrier associated with MT formation, leading to an average filament length that is significantly reduced when compared with other methods of polymerization [15]. In our experiments, the average length of GMPCPP-stabilized MTs is $1.5\,\mu m$. Short MT filaments are essential for obtaining robustly flowing active gels. Longer MTs form highly elastic gels and the force provided by the motors is not sufficient to drive them to highly non-equilibrium states [16,17]. We speculate that this is because longer stabilized MTs have greater propensity to cross-link with each other.

Adding a non-adsorbing polymer such as PEG induces an attractive interaction between MT filaments by the well-studied depletion mechanism leading to the assembly of filamentous bundles [18,19] (figure 1a). For all experiments described here, MTs are used at high concentrations at which they form a percolating three-dimensional network which structurally resembles a classic viscoelastic gel-like material. However, unlike conventional gels active gels continuously undergo an ATP-driven dynamic network remodelling.

MT-based gels are driven away from equilibrium by clusters of kinesin molecular motors, which use chemical energy from ATP hydrolysis to take discrete 8 nm steps along the MT backbone [20,21]. MTs are inherently polar filaments and the kinesin motors used in this study move specifically towards the MT plus end. Kinesin motors are labelled with a biotin linker and a tetrameric streptavidin binds several motors into multi-motor clusters (figure 1b). Such clusters can simultaneously bind and translocate along multiple MT filaments and can drive an isotropic MT suspension into a variety of defect-ridden states that are inherently far-from-equilibrium [5–7]. We expect that the activity of the motor-induced filament sliding is significantly enhanced for MTs in a bundled geometry when compared with filaments that are on average isotropic. On average, a single kinesin motor moves about a micrometre along a filament before detaching [20]. The effective motor processivity is significantly enhanced for clusters moving along bundled MTs. Even after one motor within the cluster unbinds, the cluster can remain attached to the bundle through other motors in the cluster. The bundled geometry then presents multiple binding sites to which the detached motor can quickly reattach, thus enhancing motor processivity and overall activity.

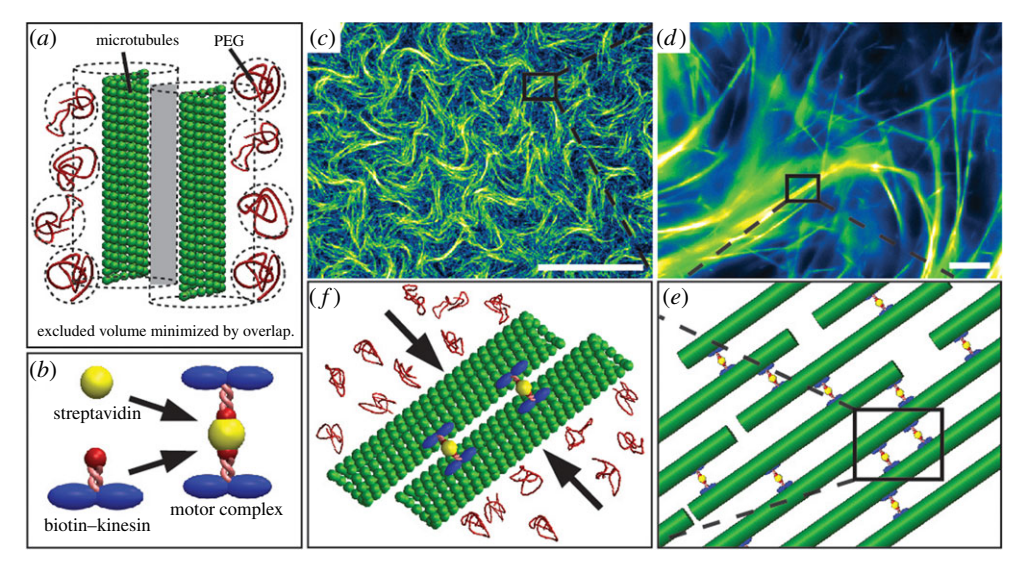


Figure 1. Deconstruction of the bundled active MT gel. (a) The active gel is composed of MT filaments which are bundled together through the depletion interaction using PEG. The depletion interaction serves to minimize the volume in the system which excludes the centre of mass of the PEG by aligning and bundling filaments along their long axis. (b) Kinesin motor complexes are assembled from biotinylated kinesin motor proteins linked together by tetrameric streptavidin. (c) A large field of view of the active gel under fluorescence microscopy shows large-scale bending of MT bundles. Scale bar is 250 μ m. (a) Zooming into a region of the gel reveals a gel structure of bundles of polydisperse size. Scale bar is 10 μ m. (a) A schematic of an MT bundle depicts many MT filaments cross-linked by the kinesin motor clusters. (a) The fundamental interactions of the primary components of the system are summarized. Filaments bundled together through depletion are cross-linked by kinesin motor complexes.

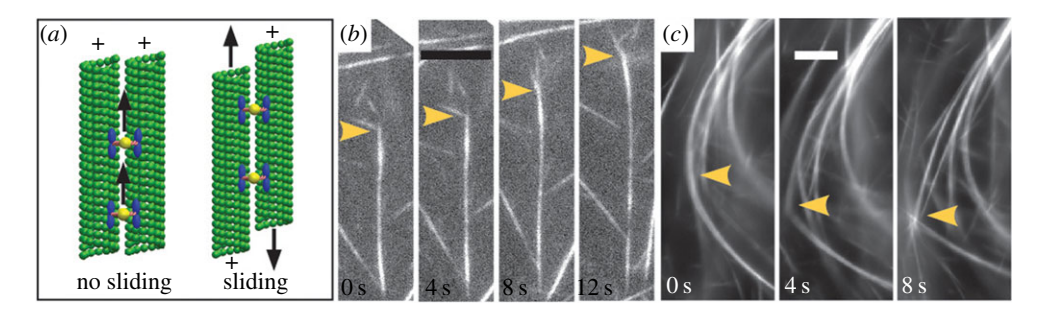


Figure 2. Bundle extension and buckling. (a) When the MTs are polarity aligned kinesin clusters processively walk towards the plus end of the bundle without inducing MT sliding. Motor clusters will induce interfilament sliding when MTs are polarity antialigned. (b) Time sequence shows that a bundle of many MTs exhibits extensile behaviour. Scale bar is 10 μ m. (c) Bundles of MTs confined in a network become sterically hindered at their ends. A time sequence shows that this extensile force leads to bundle buckling. Scale bar is 10 μ m.

The nature of the sliding force depends on the relative MT polarity in the bundle (figure 2*a*). When adjacent MTs are polarity aligned, kinesin motors will jointly walk towards the plus ends of the bundle without generating interfilament sliding [5]. By contrast, when two MTs are antialigned (MT plus ends are on distal ends), kinesin motor clusters will move towards opposite ends and cause the filaments to slide past one another. When acting on an isolated bundle, the kinesin clusters will locally polarity sort the MT filaments [22,23]. Once the bundle is polarity sorted, it remains in a quasi-static configuration as motors simply translocate along the polarity-sorted

regions without inducing any further filament sliding. Experimentally, we observe that such polarity sorting is frequently accompanied by overall bundle extension (figure 2b) [13].

The dynamics of dense percolating three-dimensional MT-bundled gels driven by kinesin clusters is considerably more complex than that of dilute isolated bundles. Similar to isolated bundles, kinesin clusters induce local MT polarity sorting. However, since each polaritysorting segment is connected to a background network, local extension leads to buckling of the composite bundled structure (figure 2c). Once the local curvature reaches a high enough magnitude the composite filamentous bundle fractures, producing shorter fragments. The typical buckling lengthscale is about a hundred micrometres, which is significantly larger than the length of the constituent 1 µm-long MTs. This demonstrates that bundle disintegration does not fragment individual MTs but only serves to break up the composite bundles held together by weak depletion interactions. Fragments produced due to self-driven buckling are quickly incorporated into the background network with random polarity. At this point, the molecular motors once again drives local polarity sorting and extension of constituent bundles. Therefore, the microscopic dynamics of active isotropic gels are driven by repetitious cascades of MT bundle polarity sorting, extension, buckling, fragmentation and subsequent recombination with the background network. The molecular motors continuously sort the MTs but due to the buckling instability the entire gel never attains a global polarity-sorted quiescent state.

The microscopic speed at which kinesin motors move along an MT backbone can be tuned by varying ATP concentrations [21]. However, simply dissolving a fixed initial amount of ATP in an active gel would lead to an undesirable situation where the motors continuously deplete the chemical fuel leading to gel dynamics that monotonically slows down for the entire duration of the experiment. Such conditions would make it impossible to prepare samples that have persistent steady-state microscopic dynamics over multiple hours required for quantitative studies. To overcome this challenge, we incorporate an ATP regenerating system into our active gel [24]. As soon as a kinesin motor hydrolyses an ATP into an ADP, pyruvate kinase/lactic dehydrogenase enzymes (PK/LDH) use energy from a high-energy chemical compound phosphoenol pyruvate (PEP) to regenerate ATP. Using such a regeneration system, it is possible to keep a fixed ATP concentration that ranges from the micromolar to the millimolar for a sufficiently long time to perform quantitative measurements. In practice, we find that MT gels with ATP regeneration can remain active for multiple days. The limiting factor appears to be protein stability as the MTs and kinesin motors start to denature at room temperature after approximately 2 days.

2. Material and methods

(a) Polymerization of microtubules

Tubulin was purified from bovine brains with two cycles of polymerization/depolymerization in 1,4-piperazindiethanesulfonic (PIPES) buffer [25]. MTs were polymerized at concentrations of 6-8 mg ml⁻¹ in an M2B buffer (80 mM PIPES, 1 mM EGTA, 2 mM MgCl2) using GMPCPP, a non-hydrolysable analogue of GTP. GMPCPP lowers the nucleation barrier and leads to polymerization of short MTs that have an average length of 1.5 μm [15]. In some experiments, MTs were labelled using Alexa 647 dye that was attached by a succinimidyl ester linker to a primary amine on the tubulin surface [26]. Tubulin suspensions were polymerized by incubating at 37°C for 30 min. Subsequently, it was allowed to sit at room temperature for an hour. Subsequently, the MT suspension was frozen at -80° C. Repeated freezing and thawing did not alter the MT length distribution (average 1.5 µm MTs). For experiments that required varying filament concentration, polymerized MTs were centrifuged for 10 min at 80 000 r.p.m. (Beckman Optima TL, TLA100.4). Supernatant was aspirated and the MTs were resuspended in M2B buffer at concentration of approximately $90 \,\mathrm{mg}\,\mathrm{ml}^{-1}$. The highly concentrated MT suspension was diluted to a final desired concentration and used within a day of polymerization.

(b) Kinesin-streptavidin motor clusters

K401-BIO-6xHIS is the 401 amino acid N-terminal domain derived from *Drosophila melanogaster* kinesin and fused to the Escherichia coli biotin carboxyl carrier protein expressed and purified from E. coli. The kinesin is also labelled with a six-histidine tag [27]. Kinesin motors were purified on a nickel column and dialysed against 50 mM imidazole, 4 mM MgCl2, 2 mM dithiothreitol (DTT), $50 \,\mu\mathrm{M}$ ATP and 36% sucrose buffer, flash frozen in liquid nitrogen and kept at $-80^{\circ}\mathrm{C}$. Thawed kinesin was mixed with tetrameric streptavidin at varying ratios in an M2B buffer solution that was supplemented with DTT. Kinesin clusters can be frozen and thawed multiple times without significant change in system activity.

(c) Poly-L-lysine—polyethylene-glycol-coated tracer beads

To suppress depletion-induced binding to network backbone, micrometre-sized polystyrene beads where coated with a polymer brush. Briefly, poly-L-lysine (PLL)-PEG block copolymer was synthesized by conjugating an N-hydroxysuccinimidyl ester of methoxypoly(ethylene glycol) propionic acid with poly-G-lysine in 50 mM sodium borate buffer, pH 8.5. The poly-lysine backbone has a positive charge that binds strongly to negatively charged polystyrene beads, leaving a brush of neutral PEG covering the bead surface. Labelling the beads was done by mixing 10 μl of PLL-PEG, 100 μl of HEPES (7.5 pH) buffer, 12 μl of stock 3 μm polystyrene beads and 878 µl of H₂O. Solution was incubated for 1 h on a rotating platform to prevent bead settling, sonicating once in every 20 min. After incubating, the beads were spun for 5 min at 4000 r.p.m., consolidated in a tube with M2B buffer, spun again and resuspended in 50 µl of M2B.

(d) Sample chambers

To suppress depletion of MTs onto surfaces, sample chambers were coated with a polyacrylyamide brush [28]. Coverslips and slide glass were sonicated in 0.5% detergent solution, followed by an ethanol bath and finally a 0.1 M KOH bath to clean and etch the glass. Slides and coverslips were then immersed in a mixture of 98.5% ethanol, 1% acetic acid and 0.5% 3-(trimethoxysilyl) propylmethacrylate and allowed to soak for 15 min so silane could coat the glass surface. Slides and coverslips were rinsed with deionized (DI) water before being immersed in 2% acrylamide monomer solution, 35 µl per 100 ml solution of tetramethylethyldiamene and 70 mg per 100 ml of ammonium persulfate were added to induce formation of polymer brush. Slides and coverslips were kept in solution for up to two weeks. Before use, they were thoroughly rinsed with DI water and dried.

(e) Protocol for assembly of active gels

Active pre-solutions (without MTs) for active gels contained ATP, anti-oxidizing agents and Trolox to avoid photo-bleaching, an ATP regeneration system based on PEP and PK/LDH, and depletant polymer PEG (20 kDa). All components were suspended in M2B buffer. The active pre-solution was prepared by dissolving: 1.33 μl of anti-oxidant stock (15 mg ml⁻¹ glucose and 2.5 M DTT), $1.33\,\mu l$ of anti-oxidant stock ($10\,\mathrm{mg\,ml^{-1}}$ glucose oxidase and $1.75\,\mathrm{mg\,ml^{-1}}$ catalase), $1.7\,\mu l$ of PK/LDH, 2.9 µl of high-salt (68 mM MgCl2 in M2B) buffer, 6 µl of trolox (20 mM) and 8 µl of PEP (200 mM). Appropriate amounts of M2B, kinesin-streptavidin clusters, and PEG were added to the active pre-solution in accordance with the experiment being performed. The total volume of the active pre-solution after mixing components was 40 µl. Final active gels were made with 4 μl of active pre-solution, 1 μl of tracer bead solution and 1 μl of MTs. The standard active gel included 3.9 µl of the kinesin-streptavidin cluster mix, 8 µl of PEG and 5.14 µl of M2B in the pre-solution before mixing with MTs and beads.

To ensure sample-to-sample uniformity and reproducibility, we prepared a large pre-solution mixture for each experiment. Samples were observed in flow cell chambers that were 18 mm

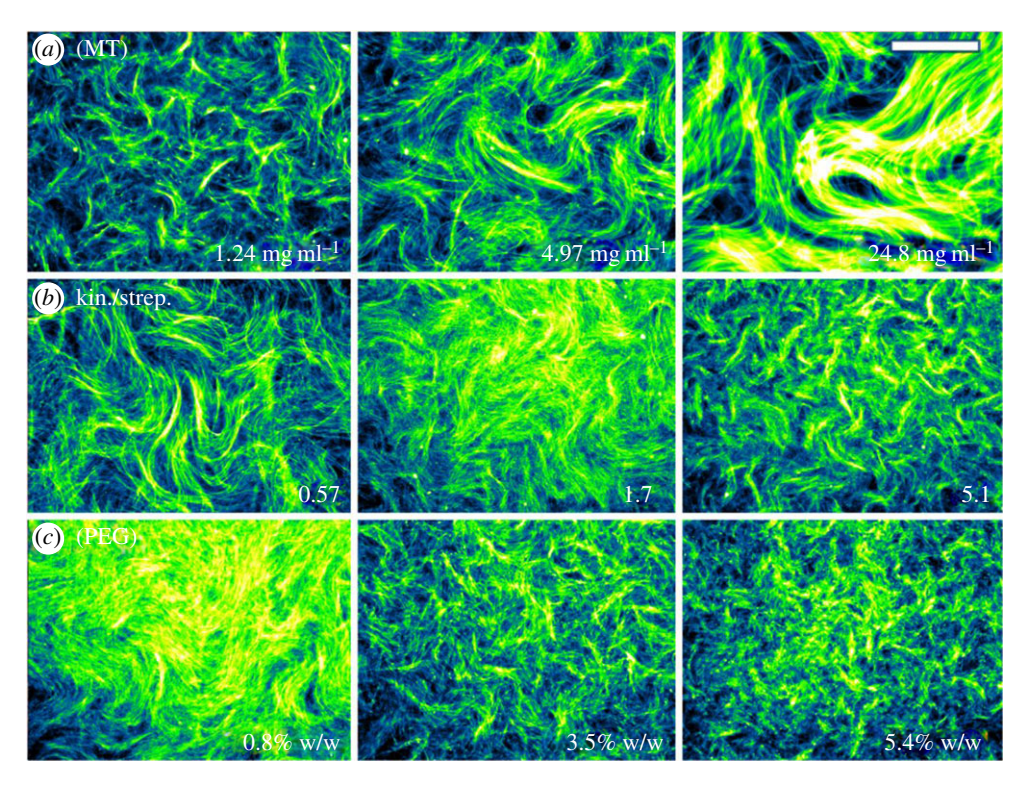


Figure 3. Gel morphology from fluorescence microscopy. (a) Influence of increasing MT concentration on the structure of the active gel. (b) Influence of increasing the ratio of kinesin to streptavidin on the structure of the active gel. (c) Influence of increasing the PEG concentration on the structure of the active gel. Scale bar, 250 μ m.

long, 2 mm wide and 100 µm deep. Data were taken at the midplane in order to minimize hydrodynamic interactions with boundary surfaces. Using fluorescence microscopy, the active gel was monitored until it reached stable activity (figure 3). Beads embedded in the active gel were imaged using brightfield microscopy with a 10× objective at frames rates that varied from 1 to 10 frames s⁻¹, depending on the apparent network speed. Bead tracking was performed using custom Matlab code based on algorithms described by Crocker & Grier [29]. From the tracked bead positions, complete particle trajectories were constructed.

Each set of experiments varied one parameter while keeping all other parameters constant. Unless otherwise indicated ATP was fixed at 1.43 μM, MTs at 1 mg ml⁻¹, active cluster concentration at 0.41 µM (mixed at a ratio of 1.7 kinesins per streptavidin) and depleting agent at 0.8% PEG (w/w).

3. Results

To quantify flow dynamics, we suspended micrometre-sized beads into active gels. Being coated with a polymer brush, the beads do not adsorb onto the MT backbone but are advected by the spontaneous flow generated by the active isotropic gel (see the electronic supplementary material, Movie S1). Quantifying bead trajectories provides information about the spatiotemporal characteristics of active flows. First, we have determined how the dynamics of emergent flows depends on ATP concentration which controls the speed at which kinesin motor clusters move along the MT [21]. The measured mean-squared displacement (MSD) of the tracer beads was highly dependent on ATP concentration (figure 4a). For a very low ATP concentration, the beads were trapped by an enveloping MT network and they exhibit sub-diffusive MSD

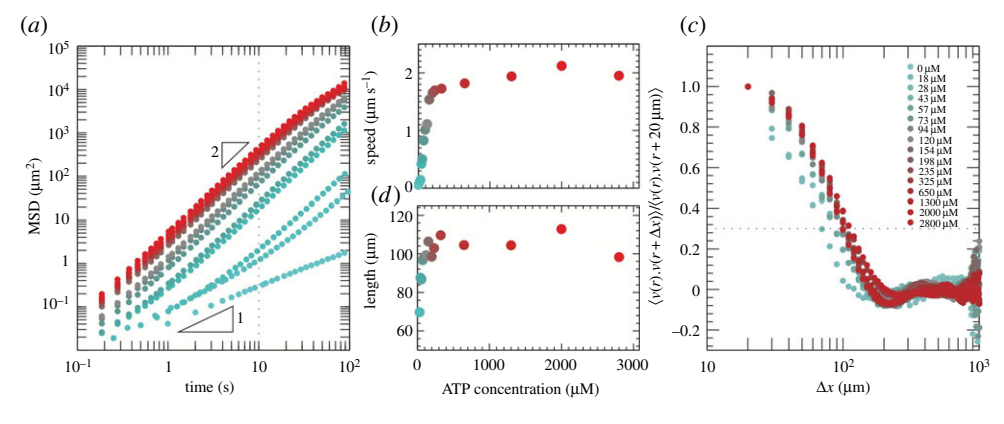


Figure 4. Tracer particle dynamics for increasing ATP. (a) Dependence of tracer particle MSDs on ATP concentration. Reference guides for a slope of 1, indicating diffusive behaviour, and a slope 2, indicating ballistic motion, are shown. The vertical dotted line indicates the time at which the characteristic speed of the tracer particles was measured. (b) Characteristic speeds of tracer particles are plotted against the concentration of ATP. (c) Normalized two-point spatial velocity—velocity correlations for tracer particles are plotted for increasing ATP concentrations. The horizontal dotted line indicates decay in correlation to 30% of the peak value and was used to measure λ the characteristic lengthscale of in the active gel. (d) Dependence of λ on ATP concentration. (Online version in colour.)

curves, a behaviour that is characteristic of conventional viscoelastic gels [30]. With increasing ATP concentration, the slope of the MSD curves gradually increased. At these intermediate ATP concentrations, the MSD curves transition from sub-diffusive to super-diffusive. In the transition region, the slope of the MSD curves is larger on longer time scales. For ATP concentrations above $28\,\mu\text{M}$, MSD curves become ballistic, indicating that the beads move essentially along straight trajectories on experimental timescales. At even longer time scales, the MSD curves will become diffusive. However, we do not have the capability to track beads for sufficiently long time to explore this regime.

Next we examined how the average network speed, defined as the average distance the beads move over 10 s, depends on the ATP concentration (figure 4b). Single molecule experiments revealed that kinesin motor speed depends on ATP concentration according to Michaelis–Menten kinetic model. In this model, the kinesin velocity is given by $v = V_{\rm max}[{\rm ATP}]/({\rm [ATP]} + K_{\rm m})$, where $V_{\rm max}$ is kinesin velocity at saturating ATP concentration and $K_{\rm m}$ is the Michaelis constant [31]. We observe that the network speed monotonically increases with increasing ATP concentration before saturating. This is in qualitative agreement with measurements for single motors. However, we note that the characteristic network speed cannot be quantitatively fitted to the Michaelis–Menten kinetics. Furthermore, for saturating conditions the average network speed is $2 \, \mu \, {\rm m \, s^{-1}}$, which is significantly faster than $V_{\rm max}$ of single kinesin which saturates at $0.8 \, \mu \, {\rm m \, s^{-1}}$. A plausible reason is that motion of multiple extensile segments within a single bundle adds up to velocities that are significantly larger than the motions of individual molecular motors.

MSD curves provide information about temporal bead dynamics. To characterize spatial variations of spontaneous flows, we have also measured normalized equal-time spatial velocity correlation functions (VCF), $\langle v(r + \Delta r)v(r)\rangle/\langle v(r)\rangle^2$, where v(r) is the velocity of a background fluid at position r (figure 4c). The measured correlation functions decay monotonically with increasing bead separation Δr . After decaying to zero they frequently become negative, indicating local rotation or vorticity within the fluid flow. Sometimes, multiple minima at larger separations are present due to multiple vortices in the field of view. From the decay of the VCF, it is possible to define the characteristic spatial flow lengthscale, λ associated with the emergent flow. With increasing ATP concentration, λ increases slightly before saturating (figure 4d). Our current hypothesis is that λ is closely linked with the buckling lengthscale of the constituent MT

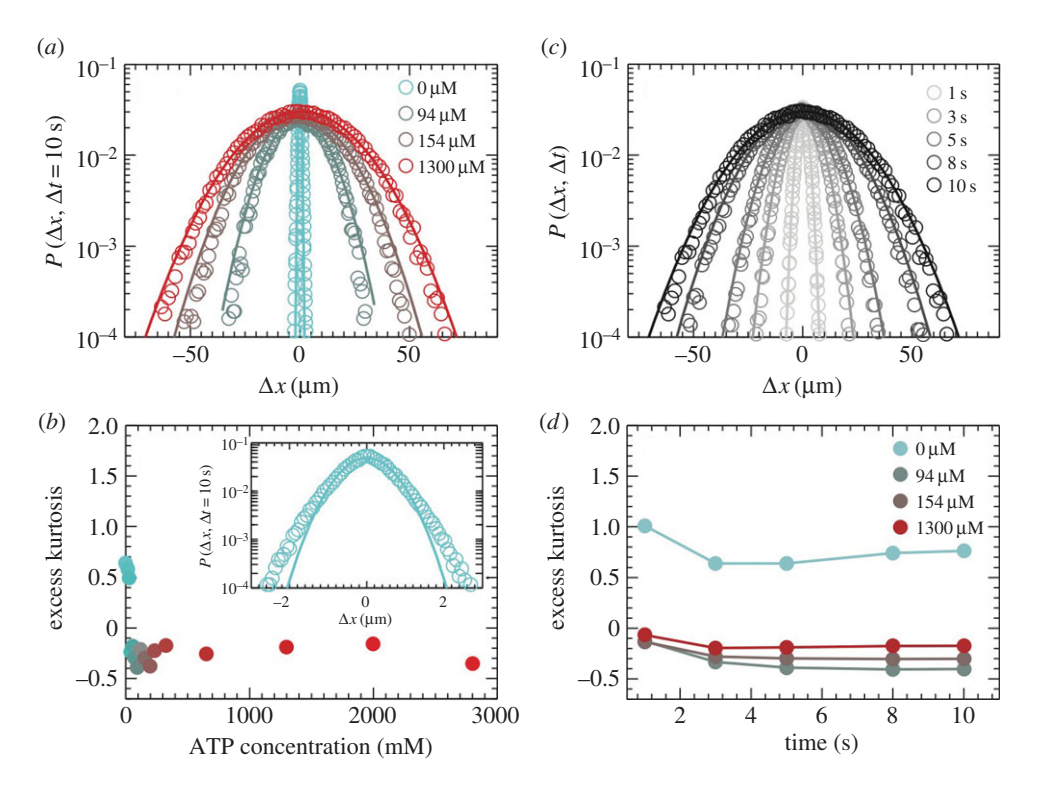


Figure 5. Displacement PDF and excess kurtosis analysis for ATP. (a) Normalized PDFs of tracer bead displacements for varying ATP concentrations, over a time step of 10 s. (b) Plot of excess kurtosis: $(u^4)/(u^2)^2 - 3$ over the range of ATP concentrations. A high kurtosis indicates a distribution that has broader tails than a Gaussian, as demonstrated in the inset graph: a blown up plot of the 0 ATP PDF at 10 s. (c) Normalized PDFs of tracer bead displacements for ATP at 1.3 mM, in the saturation range, over varying time steps. (d) Temporal evolution of excess kurtosis for a few values of ATP concentration, showing a positive value for the caged beads in the 0 ATP sample, and a negative kurtosis for active samples that tends to decrease with time step. (Online version in colour.)

bundles. However, to confirm this it is necessary to directly visualize dynamics of the constituent three-dimensional bundle network, something that has not been accomplished so far.

Besides MSD and VCF, we have further analysed the dynamics of active gels by measuring the probability density function (PDF) of the tracer particle displacements at time t given that at time t=0 the particle is located at origin. The PDF of thermally diffusing beads with no confinement is Gaussian. For conventional gels whose mesh size is comparable to the tracer size, one expects Gaussian behaviour for displacements smaller than the mesh size, but occasional 'jumps' larger than the mesh size, leading to PDF that has broader tails than those predicted by a Gaussian distribution [32]. For MT gels at zero ATP concentration we measure a similar PDF, demonstrating that they behave as conventional gels (figure 5b, inset). We quantitatively characterize the degree of Gaussianity by the distribution's excess kurtosis: $\langle u^4 \rangle / \langle u^2 \rangle^2 - 3$, where $\langle u^4 \rangle$ is the fourth moment and $\langle u^2 \rangle$ is the variance of the displacement distribution. Defined in this way, a Gaussian distribution will have an excess kurtosis of zero. An excess kurtosis of less than zero represents a distribution that has a flatter peak and narrower tails than a Gaussian. An excess kurtosis of greater than zero represents a distribution that has a sharper peak and wider tails than a Gaussian. With increasing ATP concentration, we observe a systematic trend where the Gaussian tails disappear and become narrower-than-Gaussian (figure 5a). Consequently, the excess kurtosis, which is initially larger than zero, quickly crosses zero and becomes negative (figure 5b).

We have also examined how the PDFs change with increasing time interval, t at fixed ATP concentration (figure 5c). We see two limiting behaviours depending on the activity regime. In the

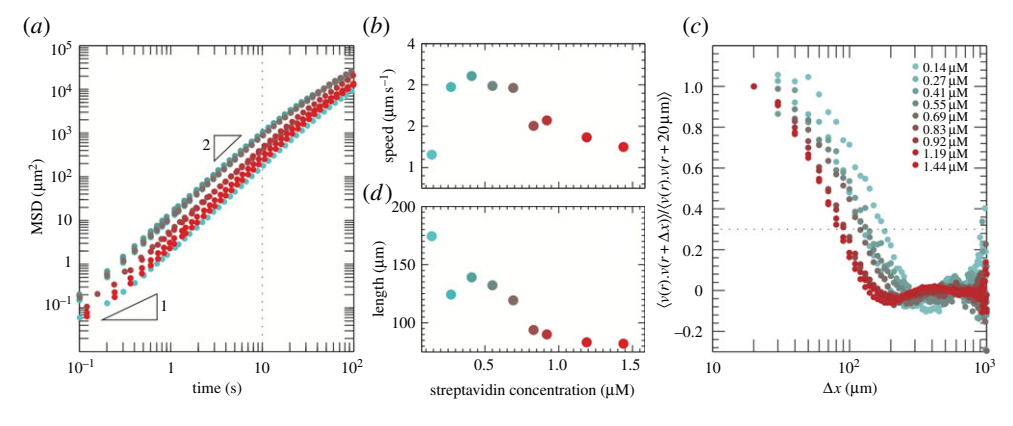


Figure 6. Tracer particle dynamics for increasing kinesin motor cluster concentration. (a) MSDs of tracer particles plotted as a function of increasing motor cluster concentrations. (b) Characteristic speeds of tracer particles are plotted against the motor cluster concentration. (c) Normalized two-point spatial velocity—velocity correlations for tracer particles are plotted for increasing cross-linker concentrations. (d) Dependence of λ on motor cluster concentration. (Online version in colour.)

equilibrium regime with zero ATP, the system exhibits 'mesh jumps' which have broader-than-Gaussian tails for all times [32] (figure 5d). For non-equilibrium regimes at higher than $56\,\mu\text{M}$ ATP concentration, the mesh is no longer well-defined, leading to an effectively Gaussian PDF for short times. This converges to a narrower-than-Gaussian PDF at long times, consistent with the concentration behaviour. We find the same generic behaviour for all gel parameters that we vary, i.e. a distribution that is narrower-than-Gaussian (negative excess kurtosis) at long times.

In suspensions of biological swimmers, one typically observes a displacement PDF that is well described by a Gaussian core with additional broader tails [33–36]. The Gaussian core arises from the thermal motion, while the hydrodynamic coupling to background swimmers leads to broader-than-Gaussian tails. The broad tail is quantified by a positive excess kurtosis which converges towards Gaussian as concentration of swimmers increases due to the superposition of many incoherent flow fields, which mimics random Brownian motion. Our system is fundamentally different from suspensions of swimmers in that we have a negative kurtosis. This negative kurtosis is manifested as a narrower-than-Gaussian tail. We hypothesize that the narrow distribution is a consequence of having relatively few active components which are large extended objects, in contrast to having many small, independent active components as in the case of swimmer suspensions. The deformation of active bundles drives large-scale flows and thus coherently moves many tracer particles with roughly the same speed, resulting in a narrower-than-Gaussian PDF.

Next we have determined how active gel dynamics depends on the concentration of kinesin motor clusters. While the MSD curves exhibited ballistic behaviour irrespective of the motor cluster concentration (figure 6a), the average gel speed exhibited interesting dependence on the same parameter. Increasing the motor cluster concentration up to $0.5\,\mu\text{M}$ increased the network speed (figure 6b). At this point, there are approximately 11 motor clusters per each MT filament. However, increasing motor cluster concentration beyond this point slowed down the network dynamics. This observation demonstrates that the fastest gel dynamics occurs for an optimal number of motors per each MT. The characteristic flow lengthscale λ also exhibited pronounced dependence on motor cluster concentration (figure 6c–d). At low motor concentrations, λ was large and it steadily decreased with increasing motor concentrations.

It is easy to understand why the network speed increases with increasing cluster concentration in the low concentration limit. For very low cluster concentration, most of the adjacent MTs will not be cross-linked by active motor clusters. Therefore, being driven by a low volume fraction of actively sliding MTs pairs, the overall extensile network dynamics will be quite slow. Increasing

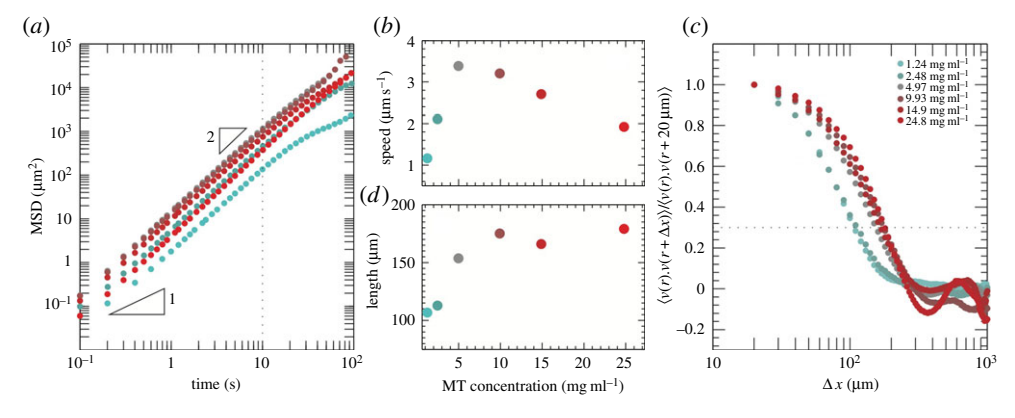


Figure 7. Tracer particle dynamics for increasing MT concentration. (*a*) Dependence of active gel MSDs on MT concentrations. (*b*) Characteristic speeds of tracer particles are plotted against the concentration of MTs. (*c*) Normalized two-point spatial velocity—velocity correlations for tracer particles plotted for increasing MT concentrations. (*d*) Dependence of λ on MT concentration. (Online version in colour.)

the cluster density increases the fraction of sliding MT pairs and thus the overall network dynamics. However, the existence of an optimal concentration of motor clusters beyond which the average speed monotonically MTs slow down is not immediately obvious. In motility assay geometry MTs slow down at high motor density for tightly coupled motors with short stalks, while for loosely coupled motors with longer stalks the MT velocity is essentially independent of the number of engaged motors [37,38]. It is also possible that in the high motor density limit there are too many kinesins per MTs which might lead to 'traffic jams' as has been seen in kinesin-8 motor systems [39,40].

Next we have studied how the active gel dynamics depends on MT concentration (see the electronic supplementary material, Movie S2). In these experiments, we increase MT concentration from 1 to 25 mg ml⁻¹, while keeping the concentration of kinesin clusters and ATP constant. We found that the MSD curves displayed ballistic behaviour for all MT concentrations examined (figure 7a). However, the average speed of the spontaneous flows exhibited a complex non-monotonic dependence on MT concentration (figure 7b). Initially, the average speed increased with increasing MT concentration reaching a maximum value of $4 \, \mu \mathrm{m} \, \mathrm{s}^{-1}$ for MT concentrations of 5 mg ml⁻¹. Increasing filament concentrations beyond this value gradually slowed the gel dynamics. Intriguingly, changing the MT concentration by more than an order of magnitude did not significantly alter the characteristic spatial flow length-scale λ (figure 7c-d). The existence of an optimum MT concentration is in qualitative agreement with the experimental observations in which we varied kinesin cluster concentration (figure 6). However, for varying MT concentration the optimal ratio of motor clusters per MT is approximately 55 which is significantly different from the optimum concentration found in figure 6. At high MT concentration, there are very few motor clusters per MT and thus the overall dynamics is very slow. With decreasing MT concentration, the motor cluster/MT ratio increases leading to increased speed of the overall network dynamics. Once past the optimal ratio of clusters/MT, there are too many molecular motors per MT and the overall dynamics slows down, similar to what is observed in figure 6.

Another parameter that critically affects the emergent dynamics of active networks is the concentration of the depleting agent (see the electronic supplementary material, Movie S3). Non-adsorbing polymer, PEG, induces attractive MT interactions and their lateral association into filamentous bundles (figure 1a). In the depletion picture, the strength of the attractive interactions is simply controlled by the PEG concentration. Below PEG concentrations of 0.6%, depletion is not strong enough to induce bundle formation and the sample remains in an

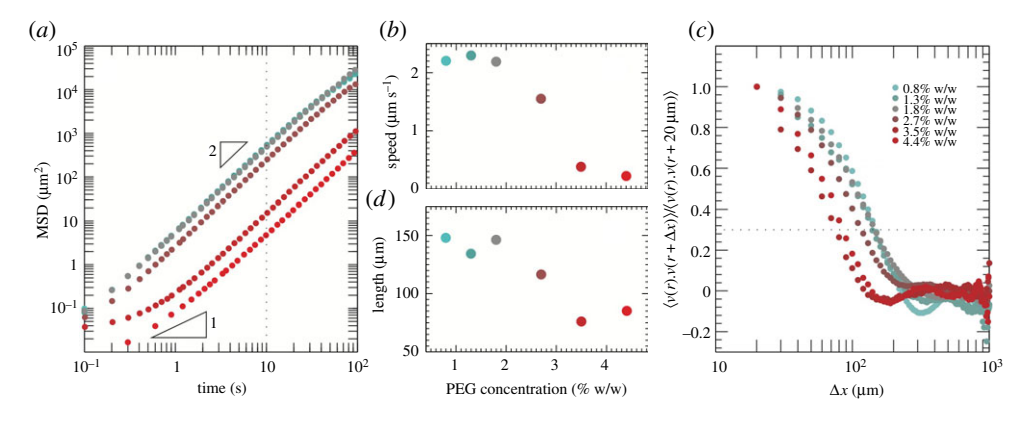


Figure 8. Tracer particle dynamics for increasing PEG concentration. (*a*) MSDs displacements of tracer particles plotted against time for increasing PEG concentrations. (*b*) Characteristic speeds of tracer particles are plotted against the concentration of PEG. (*c*) Normalized two-point spatial velocity—velocity correlations for tracer particles plotted for increasing PEG concentrations. (*d*) Dependence of λ on PEG concentration. (Online version in colour.)

isotropic state. In contrast to previous work that demonstrated formation of MT asters in mixtures of kinesin clusters and isotropic MTs [6,7], adding motor clusters to isotropic suspensions of GMPCPP MTs does not induce any large-scale dynamics. This is presumably because the average length of GMPCPP MTs is much shorter than those stabilized by taxol. Increasing the depletant concentration to 0.8% induces MT bundling and network formation which is accompanied by the emergence of spontaneous flows characteristic of active gels (figure 8a). The transition from non-bundled largely static gels at low depletant concentrations to highly dynamic gels at larger depletant concentration is very sharp. Intriguingly, this is the point at which the gel exhibits the fastest dynamics. Increasing PEG concentration beyond this value slows down the average flow speed (figure 8b). The characteristic speed at 0.8% PEG was 2 µm s⁻¹; by increasing PEG concentration to 4.4% the gel slows down to 0.3 µm s⁻¹. This trend can be perhaps understood by considering that stronger MT attractions (highest depletant concentrations) lead to increased friction associated with interfilament sliding of adjacent MTs. In this case, the motor clusters working against an enhanced load due to larger sliding friction would move at slower speeds. However, very little is known about frictional coupling between bundled filaments and how it depends on depletant concentration. The spatial flow lengthscale, λ , also exhibited strong dependence on PEG concentration, monotonically decreasing from 150 to 75 µm with increasing depletant concentration (figure 8*c*–*d*).

Finally, we varied the ratio of kinesin motors that are bound to tetrameric Streptavidin (see the electronic supplementary material, Movie S4; figure 9). While increasing the ratio of kinesin to streptavidin, the characteristic quantities behave strikingly similar to the motor concentration dependence. This is not surprising as in both cases we are manipulating the ratio of the number of kinesin motors per MT. The peak in the characteristic speed of the system occurs with a molar ratio of 1.7 kinesin per streptavidin (figure 9b); however, it should be noted that while the molar ratio suggests cluster sizes of about two motors it has been shown that clusters with upwards of eight motors are possible due to the presence of two biotin labels on each kinesin dimer [6,7].

4. Discussion

Active MT gels are intriguing far-from-equilibrium materials that exhibit macroscale spontaneous flows, enhanced transport and mixing that is driven by the coordinated motion of thousands of constituent microscopic molecular motors. All the essential microscopic ingredients of MT-based

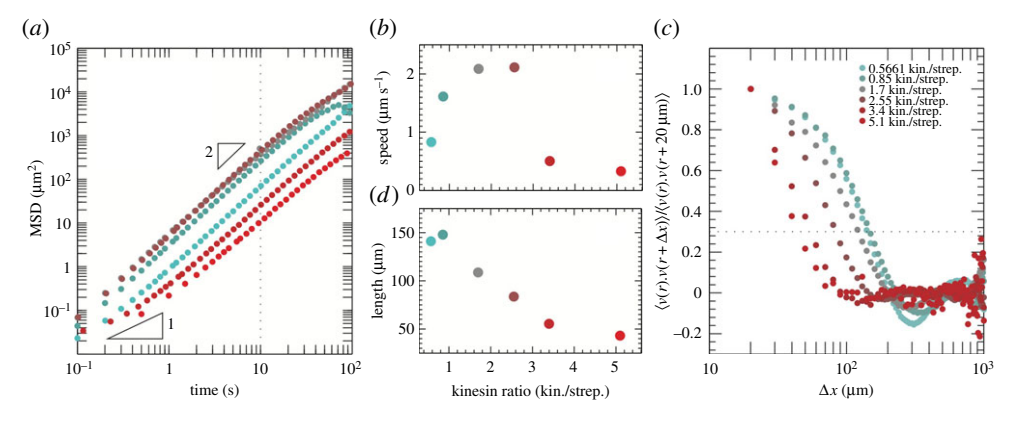


Figure 9. Tracer particle dynamics for increasing the ratio of kinesin to streptavidin. (a) MSDs of tracer for active gels with increasing kinesin to streptavidin ratio. (b) Characteristic speeds of tracer particles are plotted against the ratio of kinesin to streptavidin. (c) Normalized two-point spatial velocity—velocity correlations for tracer particles plotted as function of distance, for increasing ratio of kinesin to streptavidin. (d) Dependence of λ on kinesin to streptavidin ratio. (Online version in colour.)

active gels such as the depletion interactions, the mechanics of the constituent MT filaments or the stepping of kinesin motors have been characterized with great quantitative detail [19,41,42]. Therefore, it should be feasible to formulate theoretical models that establish a quantitative link between relevant microscopic parameters and the emergent macroscopic dynamics. However, we note that such theoretical models have not been developed so far and therefore it remains a significant challenge to explain our experimental data. At mesoscopic lengthscales, these theoretical models should also account for buckling and fragmentation of MT bundles which are held together by soft depletion interactions. These events are essential for generation of spontaneous flows at macroscopic scales. However, the mechanics of composite filamentous bundles remains a relatively unexplored area, and only recently, theoretical efforts have focused on describing certain aspects of their properties [43,44].

Being assembled from a few well-characterized components, the properties of active gels are highly controllable. For example, by controlling the ATP concentration, we tuned the speed of constituent kinesin motors from 0.1 to $1\,\mu\text{m s}^{-1}$. Furthermore, by using an ATP regeneration system, we held this motor speed constant over multiple hours allowing us to prepare and quantitatively characterize true steady-state active materials. These unique capabilities of active isotropic gels have allowed us to tune the enhanced diffusion of tracer particles over many orders of magnitude. Such enhanced diffusion is reminiscent of measurements of tracer particles in active systems that are driven by living microswimmers such as *E. coli* or *Chlamydomonas reinhardtii* [34,45,46]. However, active systems based on living organisms are not easily tunable and, consequently, the MSDs of tracer particles suspended in a bath of living swimmers usually exhibit only one type of behaviour. By contrast, the MSD curves of tracer beads suspended in active MT gels could be tuned from sub-diffusive to super-diffusive and ballistic behaviour. The divergence of an active gel from a bath of living swimmers also manifests in the kurtosis of displacement PDFs, which tend to be negative in MT gels, indicating that the flows that arise have more coherence.

Unfortunately, the parameters that we are able to tune in the bundled active MT system are not orthogonal parameters, i.e. changing one experimental parameter simultaneously changes multiple properties of active gels such as elasticity of the constituent bundle as well as their activity. For example, tuning ATP controls the speed at which kinesin motors walk along MTs and one would naively expect it to only affect the activity. However, ATP concentration also affects the motor processivity and as such it influences network elasticity. Motors act as rigid cross-linkers at low ATP concentrations, resulting in stiffer bundles. This makes even quantitative interpretation of our results difficult. Perhaps the most robust effect we have measured is a well-defined number

of motors that optimizes the overall dynamics of active gels. Increasing motor concentration beyond this limit slows down overall network dynamics (figures 6*b*, 7*b* and 9*b*).

Finally, we note that active isotropic gels are built from MT bundles, which are predominantly extensile in character. This is in sharp contrast to the other major class of biologically inspired active gels that are built from actin filaments and myosin motors, and which are always contractile [47–49]. The reason for this difference is not well understood, although it has been suggested that actin gels are contractile due to small wavelength buckling of the constituent actin filaments. MTs being orders of magnitude stiffer that actin filaments have a much longer buckling wavelength and this might suppress generation of any contractile forces [3,50].

Acknowledgements. We also acknowledge the use of Brandeis MRSEC optical microscopy facility (NSF-MRSEC-0820492).

Funding statement. This work was primarily supported by Department of Energy, Office of Basic Energy Sciences under Award DE-SC0010432TDD. Acquisition of preliminary data as well as the development of the analysis software was supported by the W. M. Keck Foundation and NSF-MRSEC-0820492.

References

- 1. Sanchez T, Welch D, Nicastro D, Dogic Z. 2011 Cilia-like beating of active microtubule bundles. *Science* 333, 456–459. (doi:10.1126/science.1203963)
- 2. Schaller V, Weber C, Semmrich C, Frey E, Bausch AR. 2010 Polar patterns of driven filaments. *Nature* **467**, 73–77. (doi:10.1038/nature09312)
- Murrell MP, Gardel ML. 2012 F-actin buckling coordinates contractility and severing in a biomimetic actomyosin cortex. *Proc. Natl Acad. Sci. USA* 109, 20820–20825. (doi:10.1073/ pnas.1214753109)
- 4. Soares e Silva M, Depken M, Stuhrmann B, Korsten M, MacKintosh FC, Koenderink GH. 2011 Active multistage coarsening of actin networks driven by myosin motors. *Proc. Natl Acad. Sci. USA* **108**, 9408–9413. (doi:10.1073/pnas.1016616108)
- 5. Hentrich C, Surrey T. 2010 Microtubule organization by the antagonistic mitotic motors kinesin-5 and kinesin-14. *J. Cell Biol.* **189**, 465–480. (doi:10.1083/jcb.200910125)
- Nedelec FJ, Surrey T, Maggs AC, Leibler S. 1997 Self-organization of microtubules and motors. Nature 389, 305–308. (doi:10.1038/38532)
- 7. Surrey T, Nedelec F, Leibler S, Karsenti E. 2001 Physical properties determining self-organization of motors and microtubules. *Science* **292**, 1167–1171. (doi:10.1126/science. 1059758)
- 8. Ramaswamy S. 2010 The mechanics and statistics of active matter. *Ann. Rev. Condens. Matter Phys.* **1**, 323–345. (doi:10.1146/annurev-conmatphys-070909-104101)
- Giomi L, Bowick MJ, Ma X, Marchetti MC. 2013 Defect annihilation and proliferation in active nematics. *Phys. Rev. Lett.* 110, 228101. (doi:10.1103/PhysRevLett.110.228101)
- Thampi SP, Golestanian R, Yeomans JM. 2013 Velocity correlations in an active nematic. *Phys. Rev. Lett.* 111, 118101. (doi:10.1103/PhysRevLett.111.118101)
- 11. Gao T, Blackwell R, Glaser M, Betterton M, Shelley M. 2014 A multiscale active nematic theory of microtubule/motor-protein assemblies. (http://arxiv.org/abs/1401.8059)
- 12. Ginelli F, Peruani F, Bar M, Chate H. 2010 Large-scale collective properties of self-propelled rods. *Phys. Rev. Lett.* **104**, 184502. (doi:10.1103/PhysRevLett.104.184502)
- 13. Sanchez T, Chen DTN, DeCamp SJ, Heymann M, Dogic Z. 2012 Spontaneous motion in hierarchically assembled active matter. *Nature* **491**, 431–434. (doi:10.1038/nature11591)
- Hyman AA, Salser S, Drechsel DN, Unwin N, Mitchison TJ. 1992 Role of GTP hydrolysis in microtubule dynamics—information from a slowly hydrolyzable analog. GMPCPP Mol. Biol. Cell 3, 1155–1167. (doi:10.1091/mbc.3.10.1155)
- 15. Sandoval IV, Weber K. 1980 Guaniosine 5'-(alpha,beta-methylene)tripohosphate enhanced specifically microtubule nucleation and stops the treadmill of tubulin protomers. *J. Biol. Chem.* **255**, 6966–6974.
- Yang YL, Lin J, Kaytanli B, Saleh OA, Valentine MT. 2012 Direct correlation between creep compliance and deformation in entangled and sparsely crosslinked microtubule networks. Soft Matter 8, 1776–1784. (doi:10.1039/c2sm06745e)
- Lin YC, Koenderink GH, MacKintosh FC, Weitz DA. 2007 Viscoelastic properties of microtubule networks. *Macromolecules* 40, 7714–7720. (doi:10.1021/ma070862l)

- 18. Needleman DJ, Ojeda-Lopez MA, Raviv U, Ewert K, Jones JB, Miller HP, Wilson L, Safinya CR. 2004 Synchrotron X-ray diffraction study of microtubules buckling and bundling under osmotic stress: a probe of interprotofilament interactions. *Phys. Rev. Lett.* **93**, 198104. (doi:10.1103/PhysRevLett.93.198104)
- Asakura S, Oosawa F. 1954 On interaction between 2 bodies immersed in a solution of macromolecules. J. Chem. Phys. 22, 1255–1256.
- 20. Vale RD, Funatsu T, Pierce DW, Romberg L, Harada Y, Yanagida T. 1996 Direct observation of single kinesin molecules moving along microtubules. *Nature* **380**, 451–453. (doi:10.1038/380451a0)
- Schnitzer MJ, Block SM. 1997 Kinesin hydrolyses one ATP per 8-nm step. *Nature* 388, 386–390. (doi:10.1038/41111)
- 22. Liverpool TB, Marchetti MC. 2003 Instabilities of isotropic solutions of active polar filaments. *Phys. Rev. Lett.* **90**, 138102. (doi:10.1103/PhysRevLett.90.138102)
- 23. Kruse K, Julicher F. 2000 Actively contracting bundles of polar filaments. *Phys. Rev. Lett.* **85**, 1778–1781. (doi:10.1103/PhysRevLett.85.1778)
- 24. Crans DC, Kazlauskas RJ, Hirschbein BL, Wong CH, Abril O, Whitesides GM. 1987 Enzymatic regeneration of adenosine 5'-triphosphate—acetyl phosphate, phosphoenolpyruvate, methoxycarbonyl phosphate, dihydroxyaceton phosphate, 5-phospho-alphea-d-ribosyl pyrophosphate, uridine-5-diphosphoglucose. *Methods Enzymol.* 136, 263–280. (doi:10.1016/S0076-6879(87)36027-6)
- 25. Castoldi M, Popova AV. 2003 Purification of brain tubulin through two cycles of polymerization-depolymerization in a high-molarity buffer. *Protein Expr. Purif.* **32**, 83–88. (doi:10.1016/S1046-5928(03)00218-3)
- 26. Sanchez T, Dogic Z. 2013 Engineering oscillating microtubule bundles. *Methods Enzymol.* **254**, 205–224. (doi:10.1016/B978-0-12-397945-2.00012-3)
- 27. Martin DS, Fathi R, Mitchison TJ, Gelles J. 2010 FRET measurements of kinesin neck orientation reveal a structural basis for processivity and asymmetry. *Proc. Natl Acad. Sci. USA* **107**, 5453–5458. (doi:10.1073/pnas.0914924107)
- 28. Lau AWC, Prasad A, Dogic Ž. 2009 Condensation of isolated semi-flexible filaments driven by depletion interactions. *Europhys. Lett.* 87, 48006. (doi:10.1209/0295-5075/87/48006)

Downloaded from https://royalsocietypublishing.org/ on 16 January 2023

- 29. Crocker JC, Grier DG. 1996 Methods of digital video microscopy for colloidal studies. *J. Colloid Interface Sci.* **179**, 298–310. (doi:10.1006/jcis.1996.0217)
- 30. Mason TG, Weitz DA. 1995 Optical measurements of frequency-dependent linear viscoelastic moduli of complex fluids. *Phys. Rev. Lett.* **74**, 1250–1253. (doi:10.1103/PhysRevLett.74.1250)
- 31. Visscher K, Schnitzer MJ, Block SM. 1999 Single kinesin molecules studied with a molecular force clamp. *Nature* **400**, 184–189. (doi:10.1038/22146)
- 32. Wong IY, Gardel ML, Reichman DR, Weeks ER, Valentine MT, Bausch AR, Weitz DA. 2004 Anomalous diffusion probes microstructure dynamics of entangled F-actin networks. *Phys. Rev. Lett.* **92**, 178101. (doi:10.1103/PhysRevLett.92.178101)
- 33. Kurtuldu H, Guasto JS, Johnson KA, Gollub JP. 2011 Enhancement of biomixing by swimming algal cells in two-dimensional films. *Proc. Natl Acad. Sci. USA* **108**, 10 391–10 395. (doi:10.1073/pnas.1107046108)
- Leptos KC, Guasto JS, Gollub JP, Pesci AI, Goldstein RE. 2009 Dynamics of enhanced tracer diffusion in suspensions of swimming eukaryotic microorganisms. *Phys. Rev. Lett.* 103, 198103. (doi:10.1103/PhysRevLett.103.198103)
- 35. Zaid IM, Dunkel J, Yeomans JM. 2011 Levy fluctuations and mixing in dilute suspensions of algae and bacteria. *J. R. Soc. Interface* **8**, 1314–1331. (doi:10.1098/rsif.2010.0545)
- 36. Saintillan D, Shelley MJ. 2012 Emergence of coherent structures and large-scale flows in motile suspensions. *J. R. Soc. Interface* **9**, 571–585. (doi:10.1098/rsif.2011.0355)
- 37. Howard J, Hudspeth AJ, Vale RD. 1989 Movement of microtubules by single kinesin molecules. *Nature* 342, 154–158. (doi:10.1038/342154a0)
- 38. Bieling P, Telley IA, Piehler J, Surrey T. 2008 Processive kinesins require loose mechanical coupling for efficient collective motility. *Embo Rep.* **9**, 1121–1127. (doi:10.1038/embor.2008.169)
- 39. Leduc C, Padberg-Gehle K, Varga V, Helbing D, Diez S, Howard J. 2012 Molecular crowding creates traffic jams of kinesin motors on microtubules. *Proc. Natl Acad. Sci. USA* **109**, 6100–6105. (doi:10.1073/pnas.1107281109)
- (doi:10.1073/pnas.1107281109)
 40. Conway L, Wood D, Tuzel E, Ross JL. 2012 Motor transport of self-assembled cargos in crowded environments. *Proc. Natl Acad. Sci. USA* **109**, 20814–20819. (doi:10.1073/

pnas.1209304109)

- 41. Gittes F, Mickey B, Nettleton J, Howard J. 1993 Flexural rigidity of microtubules and actin-filaments measured from thermal fluctuations in shape. *J. Cell Biol.* **120**, 923–934. (doi:10.1083/jcb.120.4.923)
- 42. Clancy BE, Behnke-Parks WM, Andreasson JOL, Rosenfeld SS, Block SM. 2011 A universal pathway for kinesin stepping. *Nat. Struct. Mol. Biol.* **18**, 1020–1027. (doi:10.1038/nsmb.2104)
- 43. Bathe M, Heussinger C, Claessens M, Bausch AR, Frey E. 2008 Cytoskeletal bundle mechanics. *Biophys. J.* **94**, 2955–2964. (doi:10.1529/biophysj.107.119743)
- 44. Claessens M, Bathe M, Frey E, Bausch AR. 2006 Actin-binding proteins sensitively mediate F-actin bundle stiffness. *Nat. Mater.* 5, 748–753. (doi:10.1038/nmat1718)
- 45. Chen DTN, Lau AWC, Hough LA, Islam MF, Goulian M, Lubensky TC, Yodh AG. 2007 Fluctuations and rheology in active bacterial suspensions. *Phys. Rev. Lett.* **99**, 148302. (doi:10.1103/PhysRevLett.99.148302)
- 46. Wu XL, Libchaber A. 2000 Particle diffusion in a quasi-two-dimensional bacterial bath. *Phys. Rev. Lett.* **84**, 3017–3020. (doi:10.1103/PhysRevLett.84.3017)
- Bendix PM, Koenderink GH, Cuvelier D, Dogic Z, Koeleman BN, Brieher WM, Field CM, Mahadevan L, Weitz DA. 2008 A quantitative analysis of contractility in active cytoskeletal protein networks. *Biophys. J.* 94, 3126–3136. (doi:10.1529/biophysj.107.117960)
- 48. Koehler S, Schaller V, Bausch AR. 2011 Structure formation in active networks. *Nat. Mater.* **10**, 462–468. (doi:10.1038/nmat3009)
- 49. Mizuno D, Tardin C, Schmidt CF, MacKintosh FC. 2007 Nonequilibrium mechanics of active cytoskeletal networks. *Science* **315**, 370–373. (doi:10.1126/science.1134404)
- 50. Lenz M, Thoresen T, Gardel ML, Dinner AR. 2012 Contractile units in disordered actomyosin bundles arise from F-actin buckling. *Phys. Rev. Lett.* **108**, 238107. (doi:10.1103/PhysRevLett.108.238107)